International Journal of Advance Research in Science and Engineering
Volume No 06, Special Issue No. 03, September 2017, AFM-2017
www.ijarse.com
IJARSE
ISSN: 2319-8354

Effect of Cobalt Doping on the Structural and Dielectric Properties of SnO_2 Nanoparticles

Dhanya Chandran[1], Lakshmi S. Nair[2], K. Rajendra Babu[3*] M. Deepa[4], C. M. K. Nair[5]

[1,2,3,] *Department of Physics, Mahatma Gandhi College, Kerala University, Thiruvananthapuram, (India)*

[4,5] *Department of Physics, All Saints' College, Kerala University, Thiruvananthapuram, (India)*

ABSTRACT

In this study, pure and Co doped tin oxide (SnO_2) nanoparticles were synthesized by sol-gel method and the effect of Co doping on the structural and dielectric properties were studied. The prepared samples were characterized by X-ray diffraction (XRD), X-ray Photoelectron Spectroscopy (XPS) analysis and N_2 adsorption/desorption analysis. The XRD patterns of all the samples are identified as tetragonal rutile type SnO_2 phase. The variation of dielectric constant, dielectric loss and AC conductivity of pure and Co doped SnO_2 nanoparticles are studied by varying the frequency of the applied AC signal. The AC conductivity of pure SnO_2 increases with increase in frequency but the presence of cobalt ions significantly reduced the conductivity which decreases with increase in dopant concentration.

Keywords: Band Gap Narrowing, Dielectric Constant, Sol-Gel Process, Co-Doped Tin Oxide.

I. INTRODUCTION

Tin oxide is regarded as one of the most promising semiconductors because of its unique optical, electronic and catalytic properties. They have found diverse applications in gas sensors, optoelectronic devices, solar cells, lithium-ion batteries, photocatalysis, and dye-sensitized solar cells [**1-6**]. Tin Oxide which is a wide band gap semiconductor with a band gap of 3.6 eV in its stoichiometric form shows insulating behavior, as perfectly stoichiometric samples are highly resistive. However nonstoichiometry, in particular oxygen vacancies makes it conducting [**7-8**].

In this article, pure and Co doped SnO_2 nanoparticles have been prepared through sol-gel method and the variation of dielectric constant, dielectric loss and AC conductivity of pure and Co doped SnO_2 nanoparticles are studied by varying the frequency of the applied AC signal.

II. EXPERIMENTAL

Pure and Co doped tin oxide (SnO_2) nanoparticles have been prepared by sol-gel method with different concentrations of cobalt (0.75 at%, 3 at% and 4 at%). In a typical synthesis, 5.8 g of tin (IV) chloride was

issolved in 100 ml ultra pure water and stirred for half an hour. To this solution 3.2 M ammonia solution was added drop wise under a controlled feed rate of 0.5 ml per min with constant stirring until pH 2 was reached. The sol was then kept at room temperature for 1 day to complete the ageing process. The resultant gel was washed several times with ethanol and double distilled water and dried in an oven at 80 $^{\circ}$C for 24 h. After grinding, the synthesized powder was calcined at 400 $^{\circ}$C for 2 h. Co doped SnO_2 nanopowders were prepared in a similar manner, by the addition of calculated amount of $Co(Cl)_2.6H_2O$ into $SnCl_4.5H_2O$ solution.

The dielectric measurements were carried out at room temperature over a frequency range of 42 Hz to 5 MHz using an impedance analyzer (HOIKI LCR Hi-Tester 3532-50) by applying an AC signal across the sample cell with a blocking electrode (silver) in a dielectric cell connected to the computer controlled impedance analyzer (LCR meter). The real part of the complex dielectric function was determined using the equation,

$$\varepsilon' = (Cd)/(\varepsilon_0 A) \quad (1)$$

where C is the capacitance, d is the thickness, ε_0 is the permittivity of free space and A is the area of cross-section of the cylindrical pellet.

The AC conductivity (σ_{ac}) of the samples were determined using the equation,

$$\sigma_{ac} = \varepsilon_0 \varepsilon' \omega \tan\delta \quad (2)$$

where ω is the angular frequency and $\tan\delta$ is the dielectric loss tangent.

III. RESULTS AND DISCUSSIONS

3.1. X-ray Diffraction (XRD) Analysis

The X-ray diffraction patterns of the synthesized samples were recorded with Bruker Advance diffractometer using CuKα (λ = 1.5406 Å) radiation in 2θ ranging from 20° to 80°. The XRD patterns of pure (T0), 0.75 at% Co doped (CT1), 3 at% Co doped (CT2) and 4 at% Co doped (CT3) tin oxide nanoparticles. calcined at 400 $^{\circ}$C are shown in fig.1 All the diffraction peaks can be indexed to the tetragonal rutile type SnO_2 phase and the Co doping does not change the tetragonal structure of SnO_2. The results are in good agreement with the standard JCPDS (Card No. 41-1445) data. Further, no characteristic peaks of impurities such as cobalt oxides or other tin oxides were observed in the XRD pattern showing the single phase sample formation. The average crystallite size (d) of the sample was estimated using Scherrer's equation [9]:

$$d = 0.9\lambda / \beta \cos\theta \quad (3)$$

where λ is the wavelength of the X-ray used , θ is the Bragg's angle and β is the full width at half maximum (FWHM) of the peak.

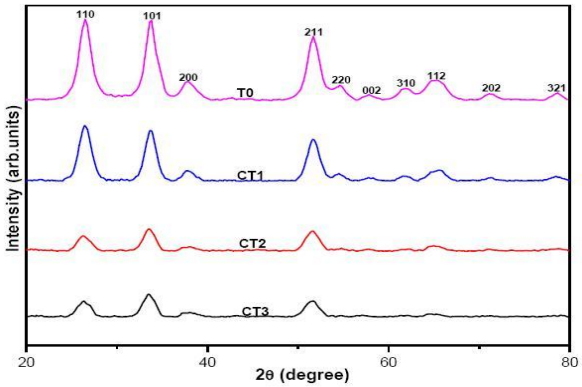

Fig. 1 XRD patterns of pure and Co doped SnO_2 nanoparticles.

The average crystallite size of the samples are given in Table 1. As compared to pure SnO_2 broadening of diffraction peaks and degradation of crystallinity can be observed with increase in cobalt content, which implies the reduction in crystallite size which is due to the distortion in the host SnO_2 lattice by Co^{2+} doping that decrease the nucleation and subsequent growth rate of SnO_2 nanoparticles [10-14]. The lattice parameters of pure and Co doped SnO_2 nanoparticles are shown in Table 1. The increase in lattice parameters with increase in cobalt concentration shows that Co ions systematically substituted Sn ions in the samples as the ionic radius of Co^{2+} (r = 0.75 Å) is larger than that of Sn^{4+} (r = 0.69 Å) [15-16].

Table 1 Comparison of particle size, lattice parameters and specific surface area of pure and Co doped SnO_2 nanoparticles.

Samples	Size from Scherrer equation (nm)	Lattice parameter a (nm)	Lattice parameter c (nm)	Specific surface area (S_{BET}) (m^2/g)
T0	6.97 ± 0.62	4.7403	3.1993	67
CT1	5.77 ± 0.18	4.7591	3.1996	97
CT2	5.13 ± 0.34	4.7821	3.2126	100
CT3	4.93 ± 0.23	4.7821	3.2254	130

3.2. X-ray Photoelectron Spectroscopy (XPS) analysis

To investigate the oxidation state and chemical composition of doped samples, X-ray Photoelectron Spectroscopy (XPS) measurements was carried out using a Kratos ESCA model AXIS 165 X-ray Photoelectron Spectrometer equipped with a Al Kα source (1486.6 eV). The XPS 3d Sn spectrum is presented in figure 2 (a) which shows two characteristic peak of Sn $3d_{3/2}$ and Sn $3d_{5/2}$ centered at 487.3 eV and 495.7 eV, respectively, with spin orbit splitting (SOS) value 8.4 eV which match with standard values of Sn^{4+} [17-18].

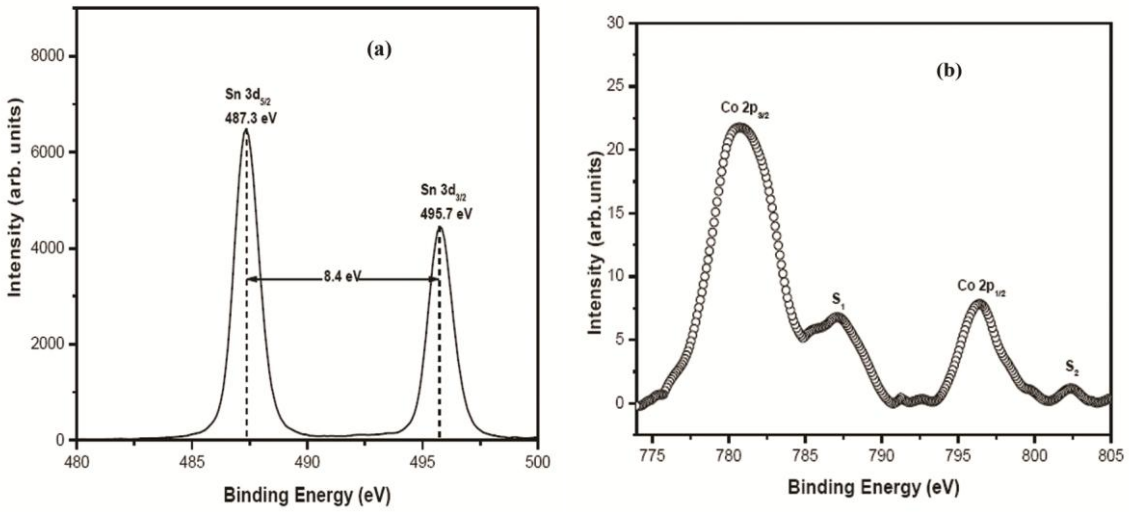

Fig. 2 XPS spectra of sample CT3: (a) Sn 3d spectrum (b) Co 2p spectrum

Figure 2 (b) shows the core-level Co 2p XPS spectrum of sample CT3 in which four broad peaks are observed in the Co 2p region. The binding energy (BE) positions of Co $2p_{3/2}$ and $2p_{1/2}$ is located at 780.7 and 796.2 eV, respectively. The energy difference between Co $2p_{3/2}$ and Co $2p_{1/2}$ is 15.5eV which confirms that Co is in +2 oxidation state as the standard spin orbit splitting value for Co^{2+} is 15.5 eV. The spectrum also exhibits two shake-up satellite peaks on higher binding energy side, represented as S_1 and S_2, centered at 786.9 and 802.3 eV and these satellite structure on high binding energy side of Co $2p_{3/2}$ and Co $2p_{1/2}$ is a typical characteristic of high-spin Co^{2+} [19-21]. Thus above findings demonstrate that Co ions is successfully incorporated as Co^{2+} in the host matrix.

3.3. Brunauer-Emmett-Teller (BET) analysis

The specific surface area of undoped and doped samples was determined from the adsorption isotherm of nitrogen at 77K on the basis of the Brunauer-Emmett-Teller (BET) method using a micrometrics Gemini 2375, after degassing the samples at 200°C for 2 hours. Fig. 3 shows the N_2 adsorption/desorption isotherms of pure and Co doped SnO_2 nanoparticles. They exhibit type IV isotherms with a H2 type hysteresis loop observed in the relative pressure (p/p_0) range of 0.45-0.95, revealing the characteristic of mesoporous materials. The specific surface areas of the prepared samples were calculated using the BET method and are given in Table 1 and it was found that the specific surface area increases with increase in Co content.

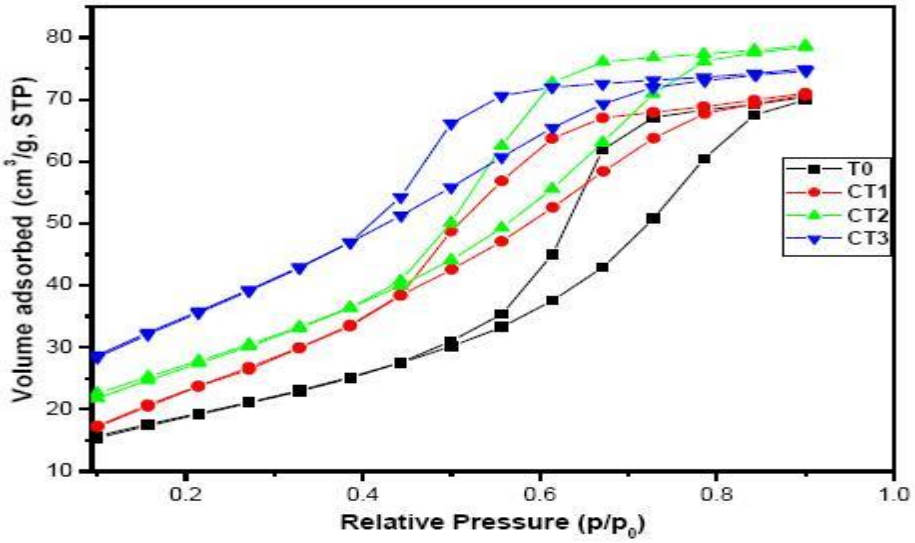

Fig. 3 Nitrogen adsorption/desorption isotherms of pure and Co doped SnO_2 nanoparticles.

3.4. Dielectric constant

Figure 4 shows the variation of real part of dielectric constant with frequency for pure and Co^{2+} doped SnO_2 nanoparticles at room temperature.

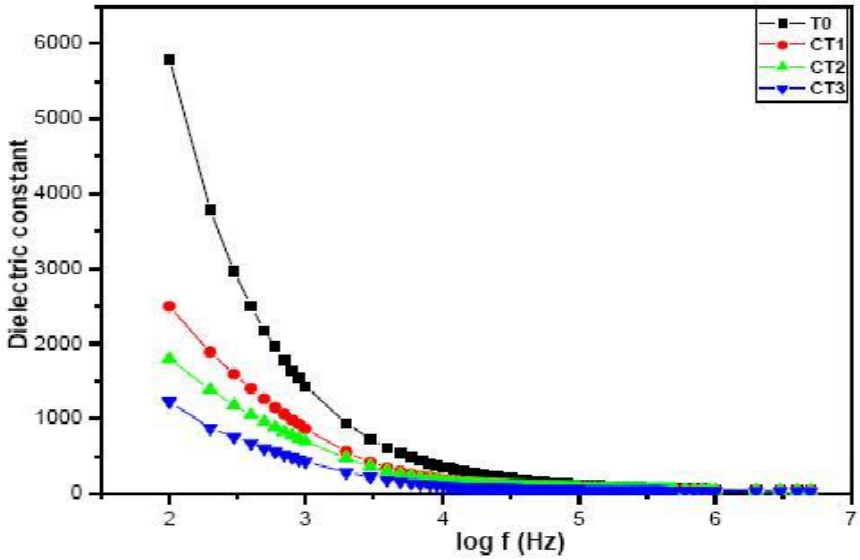

Fig. 4 Variation of real part of dielectric constant with frequency of pure and Co^{2+} doped SnO_2 nanoparticles.

It is observed that the dielectric constant decreases with increase in frequency of the applied AC signal and with increase in doping concentrations of the cobalt ions. The observed dielectric behavior can be explained on the basis of Maxwell–Wagner interfacial model [22]. At lower frequencies, the higher value of dielectric constant is due to the simultaneous presence of space charge, dipolar, ionic and electronic polarizations. The frequency

independent behavior observed in all the samples at higher frequency is due to the fact that beyond a certain frequency of external field the hopping between different metal ions (Sn^{+4}, Sn^{+2}, Co^{+2}, Co^{+3}) cannot follow the changes in the applied field causing a decrease in polarization and hence of the dielectric constant. Also the decrease in the value of dielectric constant with increase in Co dopant may be due to the small dielectric polarizability of cobalt ions (1.66 $Å^3$) as compared to tin ions (2.84 $Å^3$). As a result, more tin ions will be substituted by cobalt ions and thereby decreases the dielectric polarization, which in turn decreases the dielectric constant [23-24].

3.5 Dielectricloss

Dielectric loss (tan δ) or loss tangent represents the energy dissipation in the dielectric system. Fig 5. shows the variation in dielectric loss with frequency for pure and various concentrations of cobalt doped SnO_2 nanoparticles at room temperature.

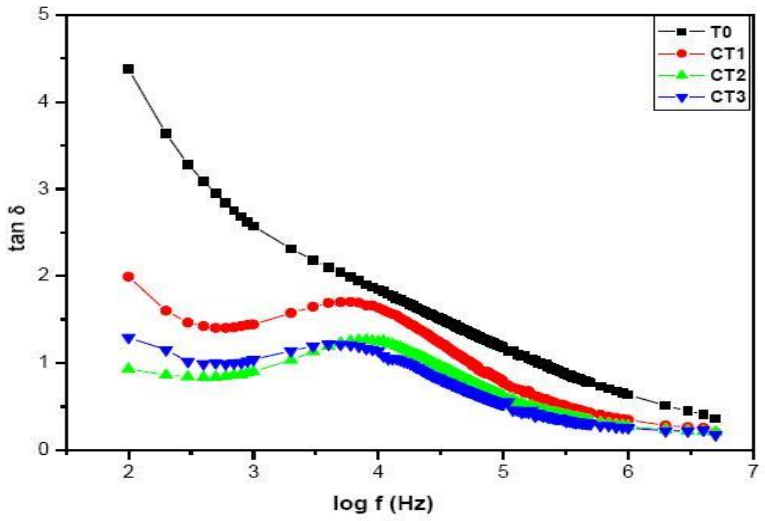

Fig. 5 Variation of dielectric loss with frequency of pure and Co^{2+} doped SnO_2 nanoparticles.

At lower frequencies the value of tan δ is large while it becomes lower at higher frequencies which is due to the dominant effect of the polarization by migrating charges at low frequency. In the case of doped samples the loss spectra were characterized by peaks at lower frequencies, represents the relaxation peaks which can occur when jumping (hopping) frequency of localized electric charge carrier becomes approximately equal to that of the externally applied ac electric field. This can be attributed to the difference in the environment surrounding various ions in a condensed material and moreover, the interactions between ions and thermal fluctuations of the lattice are not identical everywhere all time [25]. The dielectric loss decreases with increase in the frequency and becomes low at high frequency region, which shows the capability of these materials to be used in high frequency device applications.

3.6 AC conductivity

Figure 6 shows the variation of Ac conductivity (σ_{Ac}) as a function of frequency for pure and various concentrations of Co^{2+} ions doped SnO_2 nanoparticles at room temperature.

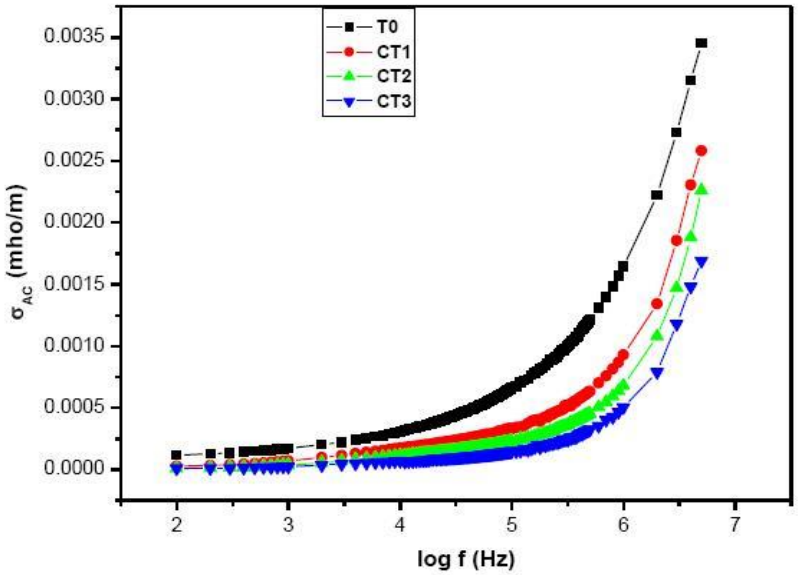

Fig. 6 Variation of ac conductivity with frequency of pure and Co^{2+} doped SnO_2 nanoparticles.

It is observed that conductivity increases as the frequency of the applied AC field increases and in all the samples AC conductivity is constant upto100 kHz and thereafter increases steeply, which is a characteristic feature of disordered materials. Also, at higher frequencies, the conductivity value decreases with increasing the concentration of cobalt ions. This is due to the fact that with increase in dopants concentration, particle size decreases and correspondingly the surface to volume ratio increases and large surface scattering occurs which results in a reduction in electronic conductivity.

At higher frequencies, the high conductivity could be attributed to short range intrawell hopping of charge carriers between the localized states occurred in a disordered manner. However, the Ac conductivity of SnO_2 was reduced by cobalt doping because the effective number of charge carriers involved in the doping mechanism was decreased and hence the conductivity was found to decrease.

IV. CONCLUSIONS

Pure and Co doped tin oxide nanoparticles were successfully synthesized by sol-gel method. The XRD study reveals that the prepared samples exhibit the rutile type tetragonal structure. The specific surface area determined from BET method was found to increase with increase in Co content. The XPS results revealed the incorporation of Co in Sno_2 lattice as Co^{2+} without forming any detectable impurity phase or Co clusters. At higher frequencies, materials showed low dielectric constant but high conductivity which makes them suitable for various dielectric applications.

V. ACKNOWLEDGEMENTS

One of the authors Dhanya Chandran acknowledges University of Kerala for financial assistance in the form of Junior Research Fellowship and the corresponding author (KRB) is greatful to KSCSTE, Govt.of Kerala for awarding the Emeritus Scientist fellowship. The authors would like to thank STIC, CUSAT, Cochin; IIT Mumbai; NIIST, Thiruvananthapuram for providing the characterization techniques.

REFERENCES

[1] Vaezi M.R and Sadrnezhaad. K (2007) Mater. Sci. Eng. B 140 73

[2] Luo L. B, Liang F. X and Jie J. S (2011) Nanotechnology 485701

[3] Birkel. A, Lee Y. G, Koll. D, Meerbeek X. V, Frank. S, Choi M. J, Kang Y. S, Char. K and Tremel.W (2012) Energy Environ. Sci. 5 5392

[4] Jiang L. Y, Wu X. L, Guo Y. G and Wan L. J 2009 J. Phys. Chem. C 113 14213

[5] Singh A.K and Nakate U.T (2013) Advan. Nanoparticles 2:66-70

[6] Duong T.T, Choi H.J, He Q.J, Le A.T, Yoon S.G (2013) J Alloy. Comp. 206–210

[7] Cullity B. D 1978 Elements of X-rayDiffraction, 2nd edn, Addison-Wesely, Massachusetts

[8] Cetin Kılıç and Alex Zunger Physical review letters 095501

[9] Rekha. K, Nirmala M, Nair M.G, Anukaliani A (2010) Phys. B. Conden. Matter 3180-3185

[10] Azam A, Ahmed A.S, Chaman M, Naqvi A.H (2010) J. Appl. Phys. 108:094329

[11] Ahmed AS, Muhamed SM, Singla ML, Tabassum S, Naqvi AH, Azam A (2011) J. Luminescence 131(1):1-6

[12] Pillai SK, Sikhwivhilu LM, Hillie TK (2010) Mater Chem Phys 619-624

[13] Karthik K, Pandian SK, Jaya NV(2010) Appl. Surf Scie 6829-6833

[14] Dhanya Chandran, Lakshmi S. Nair, S. Balachandran, K. Rajendra Babu, M. Deepa, J. Sol-Gel Sci. Technol. (2015) 582–591

[15] Entradas T, Cabrita JF, Dalui S, Nunes MR, Monteiro OC, Silvestre AJ 2014 Mater Chem. Phys 563-571

[16] Krishnakumar T, Jayaprakash R, Pinna N, Phani AR, Passacantando M , Santucci S (2009) J. Phys. Chem. Solids. 993-999

[17] Funda Aksoy Akgul, Cebrail Gumus, Ali O. Er, Ashraf H. Farha, Guvenc Akgul, Yuksel Ufuktepe , Zhi Liu. Journal of Alloys and Compounds 579 (2013) 50–56

[18] John C.Fuggle, Nils Mårtensson J. Electron Spectro. Related Phenomena 1980, 275-281

[19] Chandni Khurana, O. P. Pandey, Bhupendra Chudasam. J. Sol-Gel Sci Technol (2015) 75:424–435

[20] Kajari Das, Shailesh N. Sharma, Mahesh Kumar and S. K. De. J. Phys.Chem.C, 2009, 14783–14792

[21] N.Rajkumar and K. Ramachandran. IEEE Transac. Nanotech, 2011, 513-519

[22**]** T. Prodromakis, C. Papavassiliou**,** Appl. Surf. Sci. 2009, 6989-699415

[23] R. D. Shannon. J.Appl. Phys. (1993), 348-366.

[24] Ameer Azam, Arham S. Ahmed, M. Chaman, and A. H. Naqvi. J. Appl.Phys, (2010) 094329

[25] M. Mehedi Hassan, Wasi Khan, Ameer Azam, A.H. Naqvi J.Indust. Eng. Chem. (2015) 283–291